

Contents lists available at ScienceDirect

Lithos

journal homepage: www.elsevier.com/locate/lithos

Metamorphic P–T paths of metapelitic granulites from the Larsemann Hills, East Antarctica



Laixi Tong ^{a,*}, Xiaohan Liu ^b, Yanbin Wang ^c, Xirong Liang ^a

^a State Key Lab of Isotope Geochemistry, Guangzhou Institute of Geochemistry, Chinese Academy of Sciences, Guangzhou 510640, China

^b Institute of Tibetan Plateau, Chinese Academy of Sciences, Beijing 100085, China

^c Institute of Geology, Chinese Academy of Geological Sciences, Beijing 100037, China

ARTICLE INFO

Article history:

Received 24 March 2013

Accepted 24 January 2014

Available online 6 February 2014

Keywords:

Metamorphic P–T paths

Metapelitic granulites

Larsemann Hills

East Antarctica

ABSTRACT

Through detailed textural observations, a peak M1 assemblage garnet + orthopyroxene + cordierite + K-feldspar has been identified in a structurally early Al-rich metapelitic granulite lens from the Larsemann Hills, East Antarctica. The M1 assemblage has been overprinted by M2 cordierite corona and M3 orthopyroxene + cordierite symplectite on garnet grains. Quantitative modeling for the peak M1 assemblage via the THERMOCALC program in the KFMASH system suggests that it was formed by the crossing of the univariant reaction garnet + biotite = cordierite + orthopyroxene + K-feldspar + melt under P–T conditions of 6–8 kbar and 840–880 °C, followed by post-peak near isobaric cooling. However, the average P–T calculations for the boron-bearing pelitic granulite indicate that peak M1 conditions reached ~9.0 kbar and ~900 °C, and the overprinting M2 assemblage formed under P–T conditions of ~7.0 kbar and 800–850 °C, reflecting a post-peak near isothermal decompression. P–T estimates show that M3 conditions reached 4–5 kbar and 700–750 °C. These imply that the M1 metamorphic evolution of the region displays contrasting P–T paths, while M2 to M3 evolution indicates a decompression-cooling process. The available chronological data support that the M1 metamorphic evolution occurred during the late Proterozoic (1000–900 Ma) Grenvillian high-grade compression tectonic event (D1), and was accompanied by strong magmatism, showing a close affinity to the northern Prince Charles Mountains and the Rayner complex. However, the overprinted M2 to M3 metamorphic evolution formed during the early Palaeozoic (~530 Ma) Pan-African high-grade tectonic events (D2–D3), and was associated with an important intracontinental reworking. This study presents an example for interpreting a complex polymetamorphic history.

© 2014 Elsevier B.V. All rights reserved.

1. Introduction

The Larsemann Hills and adjacent areas occur as an important part of the early Palaeozoic (550–500 Ma) Pan-African high-grade tectonic mobile belt (the Prydz Belt) in East Antarctica (Carson et al., 1996; Dirks and Wilson, 1995; Fitzsimons et al., 1997; Hensen and Zhou, 1995; Ren et al., 1992; Zhao et al., 1992, 1995). However, until recently, a long-standing debate still exists concerning the tectonic nature of the Prydz Belt, namely whether it represents a Pan-African suture zone associated with the final assembly of east Gondwana (Fitzsimons, 2003; Fitzsimons et al., 1997; Hensen and Zhou, 1997; Zhao et al., 2003), or is a Pan-African intraplate orogen related to intracontinental reworking (Phillips et al., 2007; Wilson et al., 2007; Yoshida, 2007). This controversy resulted from the contrasting interpretations of the metamorphic P–T history of the Larsemann Hills and adjacent areas. For instance, it was thought

that decompression-dominated P–T paths in the regions evolved during a single Pan-African (~530 Ma) metamorphic event (Carson et al., 1997; Fitzsimons, 1996, 1997; Grew et al., 2006; Thost et al., 1994), but other studies suggested that the paragneisses experienced both the ~1000 Ma and the ~530 Ma high-grade metamorphic events (Dirks and Hand, 1995; Tong and Liu, 1997; Tong et al., 1998, 2002; Zhang et al., 1996). Latter suggestion is further supported by recent new SHRIMP U–Pb age data from the paragneisses in the region (Grew et al., 2012; Wang et al., 2008). Clearly, the complete P–T paths involving the ~1000 Ma and ~530 Ma events have not yet been fully sorted out for this region, even though they are critical to our understanding of the tectonic nature of the ~1000 Ma event in the Prydz Belt and the assembly process of east Gondwana.

This paper aims to clarify the complete P–T history of the Larsemann Hills via investigations into structurally early metapelitic granulites. A garnet–orthopyroxene–cordierite-bearing pelitic granulite with multiple reaction textures will be modeled using the THERMOCALC program (Powell et al., 1998) with the dataset of Holland and Powell (1998) and the model for silicate melts in the

* Corresponding author. Tel.: +86 20 38383127; fax: +86 20 85290130.
E-mail address: lxiong@gig.ac.cn (L. Tong).

KFMASH system (Holland and Powell, 2001), combined with P–T calculations through the average P–T method (Powell and Holland, 1994). Thus, P–T paths for the early ~1000 Ma event and the overprinting ~530 Ma metamorphic event are being integrated for the region. It is suggested that the M1 metamorphic event involved a contrasting process of post-peak cooling and decompression, similar to that of the northern Prince Charles Mountains and the Rayner complex, whereas the overprinting ~530 Ma metamorphic events (M2–M3) were actually resulted from an extensive intracontinental reworking.

2. Geological background

The Larsemann Hills, located in the middle part of the Prydz Bay coast, are composed mainly of upper amphibolite to granulite facies psammitic to pelitic paragneiss, mafic–felsic composite orthogneiss and Blundell Orthogneiss (970–980 Ma), with minor leucogranitic gneiss and syn- or post-tectonic granite (Fig. 1) (Carson and Grew, 2007; Grew et al., 2012). The paragneiss sequence and composite orthogneiss were also referred to as the Brattstrand Paragneiss and Søstrene Orthogneiss respectively by Fitzsimons (1997) for the metasedimentary unit and mafic–felsic metaigneous

unit in the region and adjacent areas along the Prydz Bay coast (Carson et al., 1995a; Dirks and Wilson, 1995; Fitzsimons, 1997; Grew et al., 2012; Stüwe et al., 1989; Thost et al., 1991). The paragneisses on Stornes Peninsula, Stornesbukta and Seal Cove of Mirror Peninsula contain borosilicate minerals prismatine and grandidierite (Carson et al., 1995b; Cooper et al., 2009; Grew et al., 2006, 2007; Ren and Liu, 1994; Ren and Zhao, 2004), and a sapphirine-bearing assemblage was also reported from Stornes Peninsula (Grew et al., 2006, 2007; Ren et al., 2008; Tong and Liu, 1997). The paragneisses experienced extensive partial melting and migmatization (Dirks et al., 1993), and were considered to represent part of an extensive basinal sedimentary sequence extending about 130 km from the southern Rauer Group to the Bolingen Islands (Carson et al., 1995a, 1997). The mafic–felsic orthogneisses and paragneisses were generally interpreted as tectonically interleaved Proterozoic basement and sedimentary cover sequence in the region (Carson et al., 1995a; Dirks and Hand, 1995; Dirks et al., 1993; Fitzsimons and Harley, 1991; Sheraton et al., 1984; Stüwe et al., 1989).

However, different peak metamorphic conditions were reported for the high-grade rocks in this region and adjacent areas (Table 1), and these led to distinct explanations regarding the P–T history of the Prydz Bay coast. For example, the region was initially

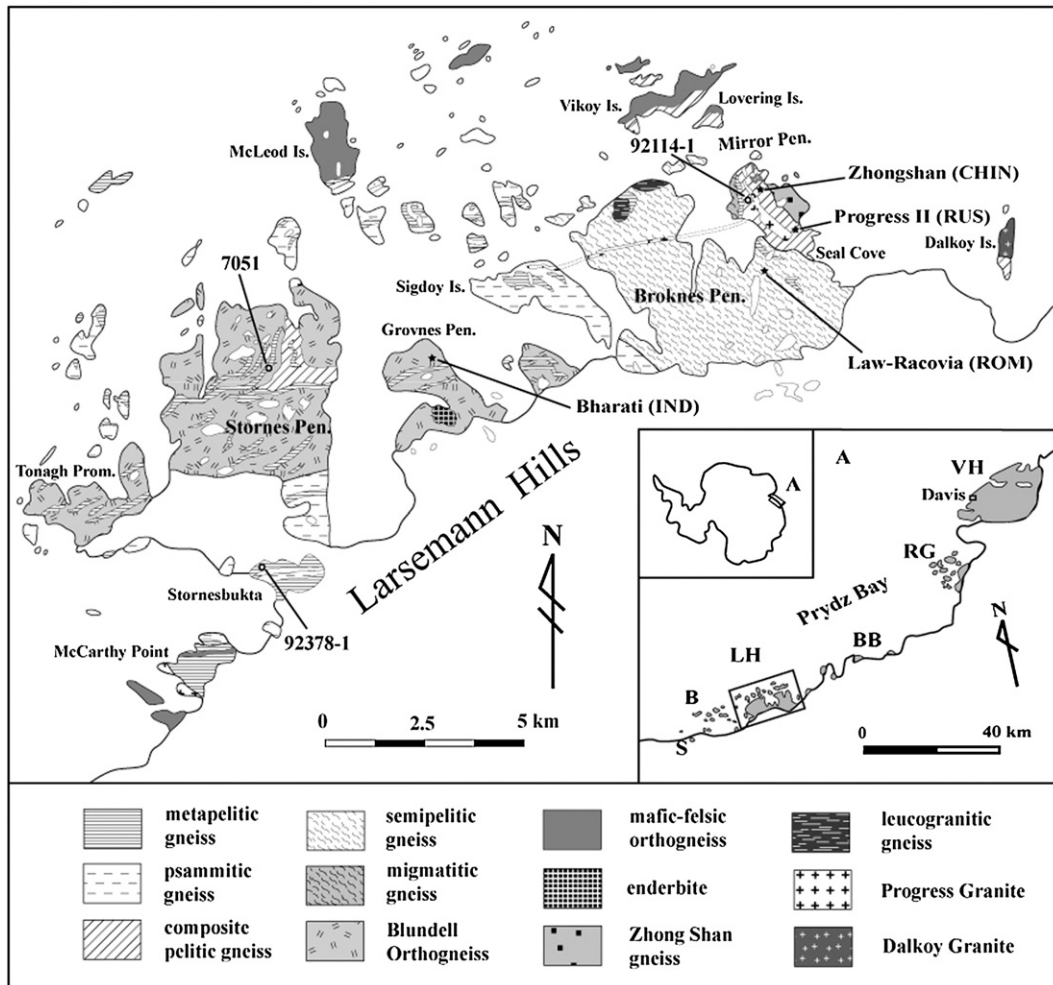


Fig. 1. Geological map of the Larsemann Hills, east Antarctica, showing the major lithological units and sample locations (after Carson and Grew, 2007; Carson et al., 1995a; Tong et al., 2002). Inserted map shows the site of the Larsemann Hills in Prydz Bay, LH, Larsemann Hills, S, Søstrene Island, B, Bolingen Islands, BB, Brattstrand Bluffs, RG, Rauer Group, VH, Vestfold Hills.

Table 1
Summary of P–T estimates and ages from the literature for the high-grade metamorphic rocks in the Larsemann Hills region.

Author	M1	Age	M2	Age	M3	Age
Stüwe and Powell (1989a)	4.5 kbar@750 °C	~1000 Ma	3.0 kbar@600 °C	~1000 Ma	Greenschist facies	~500 Ma
Ren et al. (1992)	9.0 kbar@850 °C	?	4.5 kbar@750 °C	~500 Ma	Greenschist facies	?
Tong and Liu (1997)	9.5 kbar@870 °C	~1000 Ma	–	–	–	–
Grew et al. (2006)	6–7 kbar@800–860 °C	~500 Ma	~4 kbar@ ~750 °C	~500 Ma	–	–
Author	M2	Age	M3	Age	M4	Age
Dirks and Hand (1995)	10.0 kbar@980 °C	~1000 Ma	~6.0 kbar@800 °C	~500 Ma	~4.0 kbar@ ~500 °C	~500 Ma
Carson et al. (1997)	~7.0 kbar@800 °C	~500 Ma	4.5 kbar@750 °C	~500 Ma	~3.0 kbar@ ~650 °C	~500 Ma

considered to have undergone a major low-pressure granulite facies metamorphism by Stüwe and Powell (1989a) and Ren et al. (1992). Later, some researchers thought that the region and adjacent areas experienced a single medium-pressure high-temperature metamorphic event at ~530 Ma, with a clockwise decompressional P–T path and peak conditions of 6–7 kbar and 800–860 °C, whereas the paragneiss was not affected by the ~1000 Ma metamorphic event (Carson et al., 1997; Fitzsimons, 1996; Grew et al., 2006, 2007; Thost et al., 1994). This was based on the assumption that the paragneiss precursor was deposited during the Neoproterozoic (Hensen and Zhou, 1995; Kelsey et al., 2008; Zhao et al., 1995). However, other studies suggested that some early (~1000 Ma) structural-metamorphic relics (including the paragneiss) existed with higher P–T conditions of 9–10 kbar and 850–980 °C, prior to the Pan-African event in this region and adjacent areas (Dirks and Hand, 1995; Ren et al., 1992; Tong and Liu, 1997), close to peak P–T conditions (~10 kbar and ~1000 °C) reported from adjacent areas (Harley and Fitzsimons, 1991; Hensen et al., 1995; Thost et al., 1991). Therefore, this region and adjacent areas actually experienced two major high-grade metamorphic events, an early one at ~1000 Ma, and a later one at ~530 Ma (Dirks and Hand, 1995; Grew et al., 2012; Kinny, 1998; Tong et al., 1998, 2002; Wang et al., 2007, 2008; Zhang et al., 1996).

Structural studies show that the region was affected by at least four phases of deformation (Carson et al., 1995a; Dirks and Hand, 1995; Dirks et al., 1993). As suggested by recent SHRIMP U–Pb zircon ages (Grew et al., 2012; Wang et al., 2008), D1 high-grade deformation associated with interleaving of felsic and sedimentary rocks and granulite facies metamorphism (M1) occurred at ~1000 Ma, followed by intrusion of a number of felsic and mafic intrusives at 970–980 Ma. The early D1 deformation mainly occurs as intrafolial F1 folding (Carson et al., 1995a; Stüwe et al., 1989). D2 deformation belonging to SE to NW high-grade transpression formed regional gneissic foliation S2, accompanied by granulite facies metamorphism (M2) at ~530 Ma. This was followed by D3 high-strain extensional deformation, and intrusion of granites and regional NW-trending pegmatites in the region and the other neighboring areas in Prydz Bay (Carson et al., 1995a; Dirks and Hand, 1995; Dirks and Wilson, 1995).

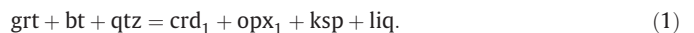
3. Field relationships and petrography

The metapelitic granulites occur as concordant layers in the D2 planar high-strain zones or lenses in low-strain zones in the study region, and they all underwent partial melting and migmatization. These metapelitic granulites generally contain coarse-grained garnet- or orthopyroxene- or cordierite-bearing peak mineral assemblages. In this study they are subdivided into three types according to their mineral assemblages: (1) orthopyroxene–prismatine–cordierite-bearing metapelitic granulite (sample 7051); (2) garnet–orthopyroxene–cordierite-bearing metapelitic granulite (sample 92378-1); and (3) garnet–orthopyroxene-

bearing but cordierite-absent metapelitic granulite (sample 92114-1).

Sample 7051 is a coarse-grained boron-bearing anatectic metapelitic granulite, occurring as a 2–5 m thick and 0.5–1.0 km long layer in a D2 low-strain zone on Stornes Peninsula (Fig. 1), with coarse-grained leucosome accounting for about 40% in volume. The less-deformed features suggest that the coarse-grained orthopyroxene–cordierite-bearing mineral assemblage is a texturally equilibrated peak assemblage. The sample consists mainly of orthopyroxene (~15%), prismatine (15%), cordierite (30%), plagioclase (25%), biotite (7–8%), K-feldspar (~5%), grandierite (~5%), quartz (~5%), and minor magnetite and hercynite, together with trace amounts of gedrite and sapphirine. The large orthopyroxene contains inclusion assemblages composed of magnetite–hercynite, whereas sapphirine and quartz may constitute part of the post-peak assemblage (Fig. 2a). Some finely segregated orthopyroxene lamellae in the orthopyroxene porphyroblast are also observed (Fig. 2a). Late biotite–magnetite symplectite occurs on the large orthopyroxene porphyroblast, and separates the orthopyroxene and cordierite (Fig. 2b). Prismatine and grandierite occur in coarse-grained cordierites. In addition, no garnet is observed in this sample.

Sample 92378-1 is a garnet–orthopyroxene–cordierite-bearing metapelitic granulite occurring as a structurally early lens within the felsic paragneiss in a D2 planar high-strain zone on Stornesbukta (Fig. 1). Its occurrence is similar to that of the garnet–orthopyroxene-bearing felsic paragneiss reported by Carson et al. (1997) from Lovering (formally Foxtrott Oskar) Island (Fig. 1). This metapelitic granulite is composed of garnet (~10%), cordierite (~10%), orthopyroxene (~15%), K-feldspar (15–20%), biotite (10–15%), quartz (~30%), plagioclase (~5%), and accessory zircons, monazite and apatite. The textural observations show that coarse-grained orthopyroxene, K-feldspar and cordierite occur between garnet porphyroblasts and quartz grains, while orthopyroxene, K-feldspar and quartz contain biotite inclusions, suggesting that the M1 peak assemblage consists of an assemblage garnet–cordierite–orthopyroxene–K-feldspar–quartz associated with a melt phase (Fig. 2c). Due to the absence of sillimanite, it is inferred that the peak M1 assemblage may have formed through a prograde biotite–dehydration partial melting reaction in the KFMASH system (Fig. 3) as follows:



Subsequent cordierite or orthopyroxene occurs as coronas around garnet grains, indicative of an M2 mineral assemblage cordierite₂–orthopyroxene₂ (Fig. 2d & e). The M2 assemblage may be inferred to have formed by another metamorphic reaction as follows:



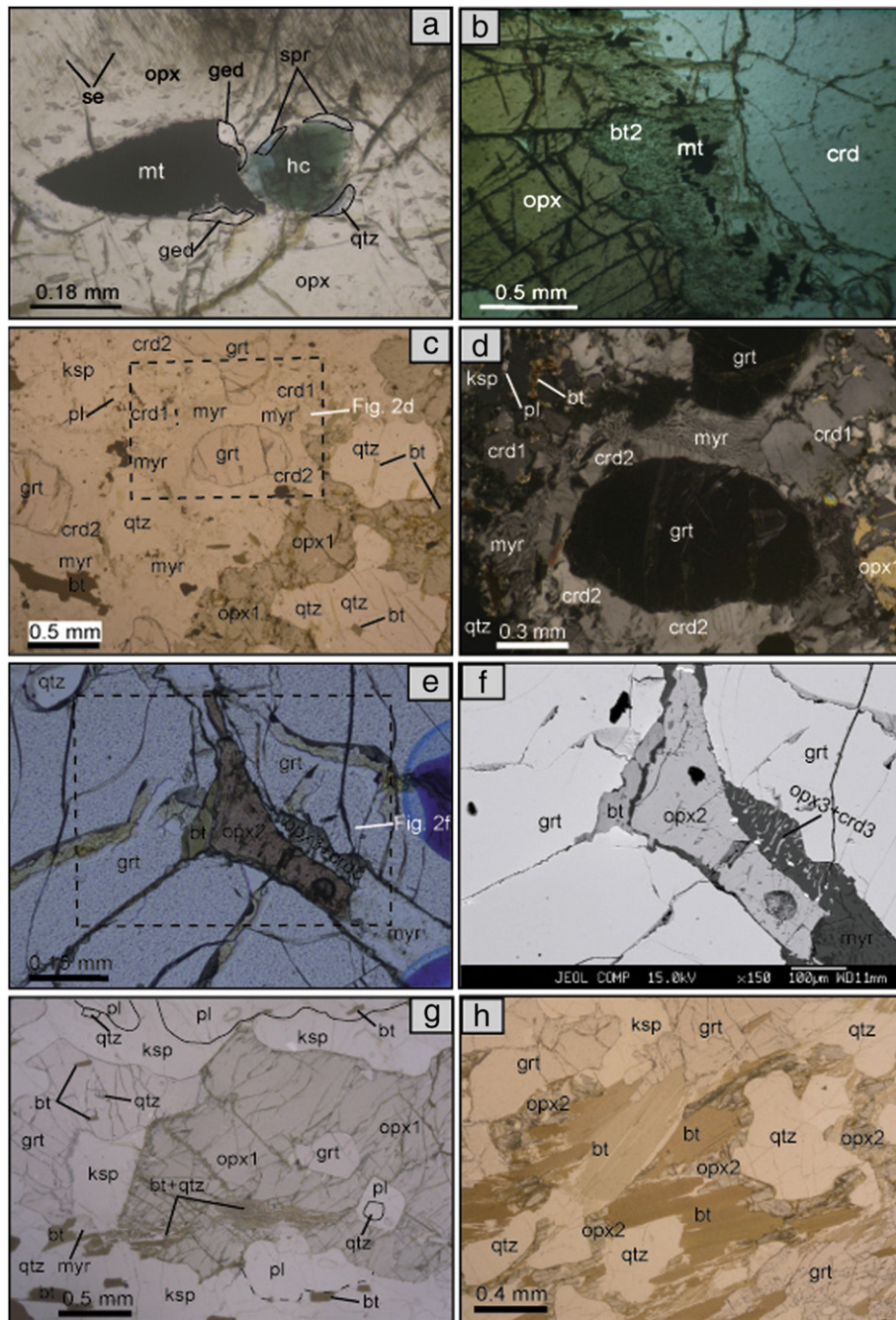
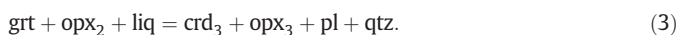


Fig. 2. Microphotographs of representative reaction textures preserved in the metapelitic granulites. (a) Sapphirine-bearing prismatine-orthopyroxene-cordierite granulite, showing large Al-rich orthopyroxene contains assemblage gedrite-magnetite or sapphirine-hercynite-quartz, and finely segregated orthopyroxene lamellae (se), sample 7051; (b) Late fine-grained biotite-magnetite symplectite around orthopyroxene porphyroblast, sample 7051; (c) Peak assemblage garnet-cordierite-orthopyroxene-K-feldspar-quartz with small pre-peak biotite inclusions, and secondary cordierite coronas (crd₂) on garnet and myrmekite, sample 92378-1; (d) Crossed polar photo of the central part of (c), showing second cordierite coronas (crd₂) on garnet; (e) Local cordierite + orthopyroxene corona (crd₃ + opx₃) on garnet, sample 92378-1; (f) Back scattered image of the central part of (e); (g) Garnet, plagioclase and quartz inclusions in orthopyroxene and small biotite and quartz inclusions in garnet, and plagioclase-quartz myrmekite adjacent to K-feldspar and biotite-quartz aggregate on biotite flake, sample 92114-1; (h) Orthopyroxene overgrowth on biotite flakes, sample 92114-1. Abbreviations: opx, orthopyroxene; crd, cordierite; spr, sapphirine; ged, gedrite; hc, hercynite; mt, magnetite; se, orthopyroxene needle; qtz, quartz; grt, garnet; bt, biotite; ksp, K-feldspar; pl, plagioclase; myr, myrmekite.

Local fine-grained cordierite-orthopyroxene symplectite (0.05–0.12 mm across) also occurs on the garnet grains, supporting the existence of an M3 assemblage cordierite₂-orthopyroxene₂ (Fig. 2e & f). The M3 symplectite appears to have formed at the expense of garnet through the following melt-consuming reaction:



Widespread myrmekitic textures (0.05–0.13 mm in width) on the margins of K-feldspars consist of a fine-grained assemblage plagioclase-quartz (Fig. 2d & f), while late biotite-quartz aggregates occur on biotite flakes. These textures suggest the presence of late transient changes in the water activity following melt crystallization probably related to M3 retrograde metamorphism.

Sample 92114-1 is a gray, massive, garnet-orthopyroxene-bearing but cordierite-absent metapelitic granulite in a layer 20–30 cm across

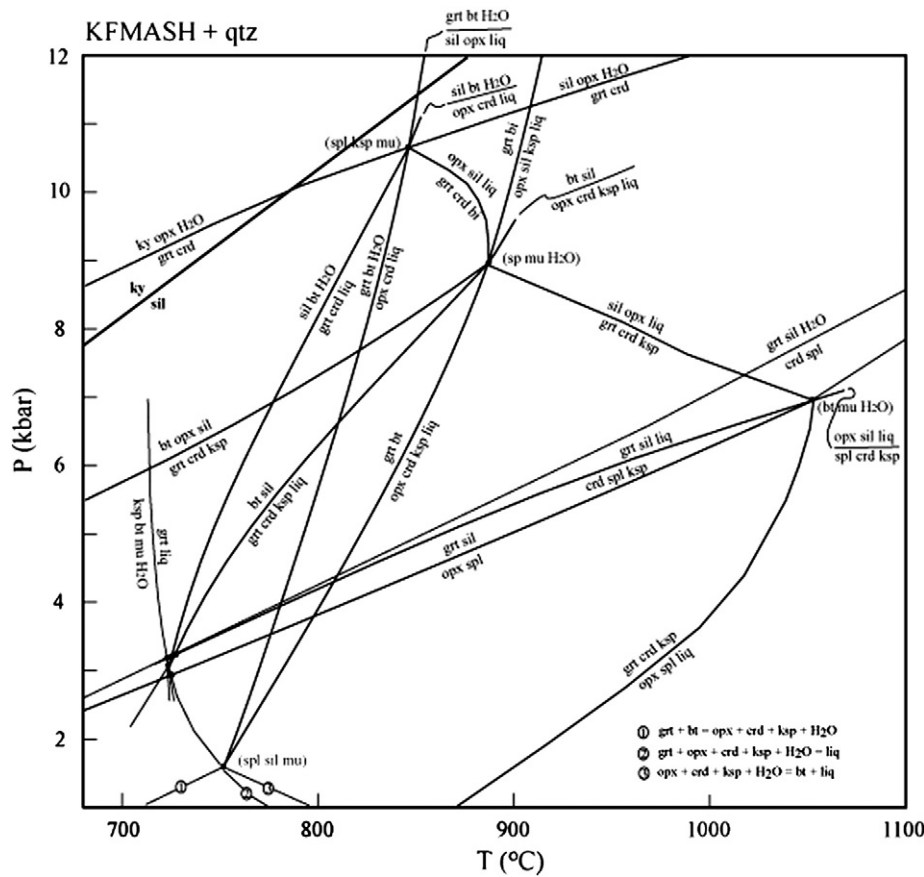
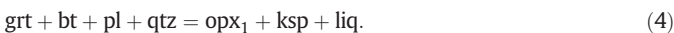


Fig. 3. P–T projection in the KFMASH model system for the metapelites of all bulk compositions, with quartz as an excess phase (after White et al., 2001).

and 40–50 m long from a D2 planar high-strain zone on the northern Mirror Peninsula (Fig. 1). This metapelitic granulite layer is interlayered with sillimanite-bearing metapelitic gneiss. The sample consists mostly of medium- to coarse-grained garnet (~15%), orthopyroxene (~15%), K-feldspar (~20%), plagioclase (~20%), biotite (~15%), quartz (~10%), minor hercynite and magnetite (<5%), and accessory zircon, monazite and apatite. The observed textures show a coexistence of coarse-grained garnet and orthopyroxene porphyroblasts with K-feldspars (0.2–0.5 mm in width) and plagioclase, which occur on the garnet and orthopyroxene grains (Fig. 2g). The garnet contains small biotite and quartz inclusions, while the orthopyroxene carries garnet, plagioclase and quartz inclusions (Fig. 2g). The textural relations indicate that the M1 peak assemblage is garnet–orthopyroxene–K-feldspar–plagioclase–biotite–quartz (Fig. 2g), whereas K-feldspar implies that a melt phase was involved at the M1 metamorphic peak. Due to the absence of sillimanite and cordierite, the textures suggest that a prograde partial melting reaction may have occurred as follows:



In addition, orthopyroxene occurs as a mantle around the peak biotite flakes, and separates peak quartz grains and biotite flakes, indicating that the orthopyroxene mantle represents an M2 assemblage (Fig. 2h). Therefore, such a texture suggests a decompression-generated partial melting reaction associated with M2 metamorphism, such as:



Similar orthopyroxene mantles around biotite flakes have also been reported from the Rauer Group (Tong and Wilson, 2006). As in sample 92378-1, the late myrmekite assemblage plagioclase–quartz on the margins of K-feldspars and biotite–quartz aggregate on biotite flakes also occur in the sample 92114-1, and are probably related to the M3 retrograde metamorphism.

4. P–T estimates

Presentation of electron microprobe data of mineral compositions for representative samples and discussion of mineral chemical compositions are given in Appendices A and B. Through applying the average P–T calculation method of Powell and Holland (1994) and the THERMOCALC program (Powell et al., 1998), combined with changes of water activities, P–T estimates for M1 peak mineral assemblages and M2 assemblages in the studied samples have been undertaken. The results for the representative samples are listed in Tables 2 and 3. As late M3 assemblages are not sufficient to apply the average P–T method, garnet–orthopyroxene pair thermobarometry is applied for M3 P–T estimates, and the results are listed in Table 3.

Sample 7051: The Al-rich core of orthopyroxene porphyroblast in this sample is inferred to have formed during M1 peak metamorphism. Thus, it can be used to recover M1 peak conditions. From Al-rich orthopyroxene core compositions and other texturally-equilibrated peak mineral compositions, the average pressure calculations with respect to water activities show that M1 peak pressure reached ~9 kbar at $a_{\text{H}_2\text{O}} = 0.3\text{--}0.5$ and $T = 900^\circ\text{C}$ (7051a in Table 2). As the volume of

Table 2

Average pressure calculations for peak M1 assemblages in samples 7051a, 92378-1a and 92114-1a using the approach of Powell and Holland (1994). All the fit values suggest that average pressure calculations fall within 95% confidence level.

(a) Sample 7051a: M1 assemblage												
Endmember	en	fs	mgts	crd	fcrd	phl	ann	san	q			
Activity(<i>a</i>)	0.360	0.089	0.087	0.780	0.018	0.300	0.0047	1.0	1.0			
$\sigma(\ln a)$	0.123	0.295	0.250	0.100	0.450	0.150	2.1280	0.0	0.0			
Independent reaction	1) 2mgts + 3q = crd 2) 6mgts + 2ann + 9q = 3fcrd + 2phl 3) 6mgts + 2ann + 15q = 3en + 3fcrd + 2H ₂ O + 2san											
Average pressure($a_{\text{H}_2\text{O}} = 0.3$)						Average pressure($a_{\text{H}_2\text{O}} = 0.5$)						
All endmember						All endmember						
T(°C)	850	900	950				T(°C)	850	900	950		
P(kbar)	9.7	8.7	7.3				P(kbar)	10.1	9.1	8.1		
σ	1.1	1.1	1.2				σ	1.1	1.1	1.2		
σ_{fit}	0.0	0.1	0.1				σ_{fit}	0.0	0.1	0.1		
(b) Sample 92378-1a: M1 assemblage												
Endmember	py	alm	en	fs	mgts	crd	fcrd	phl	ann	east	san	q
Activity(<i>a</i>)	0.040	0.240	0.290	0.130	0.054	0.610	0.0590	0.110	0.039	0.021	1.0	1.0
$\sigma(\ln a)$	0.390	0.154	0.151	0.245	0.354	0.101	0.3440	0.268	0.393	0.439	0.0	0.0
Independent reaction	1) 4py + 2alm + 9q = 6en + 3fcrd 2) 2py + 4alm + 9q = 6fs + 3fcrd 3) 2alm + 6mgts + 9q = 2py + 3fcrd 4) 2alm + en + 3q = 3fs + crd 5) 2en + east = py + phl 6) fs + 2fcrd + 2ann = 4alm + 2san + 2H ₂ O 7) 15en + 6fcrd + 6east = 14py + 4alm + 6san + 6H ₂ O 8) 3en + 6fcrd + 2ann = 2py + 10alm + 6san + 6H ₂ O											
Average pressure($a_{\text{H}_2\text{O}} = 0.3$)						Average pressure($a_{\text{H}_2\text{O}} = 0.5$)						
All endmember						All endmember						
T(°C)	900	950	1000				T(°C)	900	950	1000		
P(kbar)	6.1	6.5	6.9				P(kbar)	6.2	6.5	6.8		
σ	1.0	1.2	1.5				σ	1.0	1.2	1.5		
σ_{fit}	1.5	1.9	2.3				σ_{fit}	1.9	1.5	1.8		
(c) Sample 92114-1a (M1):				$a(\text{H}_2\text{O}) = 0.3$				$a(\text{H}_2\text{O}) = 0.5$				$a(\text{H}_2\text{O}) = 0.7$
Activity(<i>a</i>)				T = 750 °C				T = 800 °C				T = 850 °C
py(0.012) gr(0.00022) alm(0.37)				avP = 6.1 kbar				avP = 6.5 kbar				avP = 7.0 kbar
en(0.23) fs(0.17) mgts(0.0014)				sd = 1.6				sd = 1.9				sd = 2.1
phl(0.17) ann(0.0138) east(0.021)				fit = 1.49				fit = 1.64				fit = 1.77
an(0.59) san(1.0) qtz(1.0)												

leucosome reaches ~40% in this sample, a higher $a_{\text{H}_2\text{O}}$ is preferred here for this sample. Thus, M1 peak pressure will be ~9 kbar at $a_{\text{H}_2\text{O}} = 0.5$ and $T = 900$ °C. Accordingly, the low-Al rim of orthopyroxene porphyroblasts is inferred to have formed during post-peak M2 metamorphism. Using the orthopyroxene rim compositions and texturally-equilibrated other mineral compositions, the average pressure calculations indicate that M2 pressure attained 6–7 kbar at $a_{\text{H}_2\text{O}} = 0.3$ –0.5 and $T = 850$ °C (7051b in Table 3). These results are compatible with the M2 peak conditions of ~7 kbar and 800 °C reported by Carson et al. (1997).

Sample 92378-1: Using M1 garnet core compositions and texturally-equilibrated other peak mineral compositions in this sample, the average pressure calculations with respect to water activities indicate an M1 pressure range of 6.1–6.2 kbar at $a_{\text{H}_2\text{O}} = 0.3$ –0.5 and $T = 900$ °C (92378-1a in Table 2). From the garnet rim composition, the X_{Mg} -rich cordierite corona and texturally-equilibrated mineral compositions, the average pressure calculation results show an M2 peak pressures range of 6.4–6.5 kbar at $a_{\text{H}_2\text{O}} = 0.3$ –0.5. For instance, the calculation shows $P = 6.5 \pm 1.2$ kbar at $a_{\text{H}_2\text{O}} = 0.3$ and $T = 850$ °C (92378-1b in Table 3). The above average pressure calculations indicate a near-

isobaric cooling process from peak M1 to M2. This is consistent with the calculated phase diagram as shown in the P–T pseudosection, which suggests that the X_{Mg} -rich M2 cordierite corona should have formed through a cooling process accompanied by a slight increase in pressure (see next section).

Sample 92114-1: The average pressure calculations regarding water activities from texturally-equilibrated M1 peak assemblages give $P = 6.0$ –6.5 kbar at $a_{\text{H}_2\text{O}} = 0.3$ –0.5 and $T = 750$ –800 °C (92114-1a in Table 2). The pressure calculations for equilibrated post-peak M2 assemblages give $P = 6.5$ –6.8 kbar at $a_{\text{H}_2\text{O}} = 0.3$ –0.5 and $T = 850$ –900 °C (92114-1b in Table 3). The generally lower pressure estimates for M1 peak assemblage in this sample may be associated with re-equilibration of Fe–Mg exchange in the minerals during cooling.

The P–T conditions of M3 retrograde metamorphism can be calculated from garnet–orthopyroxene pair thermobarometers for the M3 orthopyroxene and its contact garnet. The P–T estimate results show that the M3 P–T conditions reached 4–5 kbar and ~700 °C (Table 3). These approximate the conditions that result in partial melting to form granite at low pressure conditions, which may be

Table 3

Average pressure calculation results for the M2 assemblages in the three samples using the approach of Powell and Holland (1994). All the fit values suggest that average pressure calculations fall within 95% confidence level. P–T estimate results are also shown for M3 assemblages in the sample 92378-1. Abbreviations: G96, Ganguly et al. (1996); NG85, Nickel and Green (1985); BK90, Brey and Kohler (1990).

Sample	Activity(a)	$a(\text{H}_2\text{O}) = 0.3$	$a(\text{H}_2\text{O}) = 0.5$	$a(\text{H}_2\text{O}) = 0.7$				
7051b(M2)		T = 850 °C	T = 850 °C	T = 850 °C				
en(0.40) fs(0.089) mgts(0.057)		avP = 6.0 kbar	avP = 6.8 kbar	avP = 7.2 kbar				
crd(0.72) fcrd(0.03) phl(0.51)		sd = 1.3	sd = 1.2	sd = 1.2				
ann(0.013) east(0.045)		fit = 0.51	fit = 0.20	fit = 0.20				
san(1.0) qtz(1.0)		T = 850 °C	T = 875 °C	T = 900 °C				
92378-1b(M2)		avP = 6.5 kbar	avP = 6.4 kbar	avP = 6.8 kbar				
py(0.034) alm(0.28) en(0.29)		sd = 1.2	sd = 1.3	sd = 1.6				
fs(0.13) mgts(0.054) crd(0.70)		fit = 1.98	fit = 2.08	fit = 2.44				
fcrd(0.033) san(1.0) qtz(1.0)		T = 850 °C	T = 900 °C	T = 900 °C				
92114-1b(M2)		avP = 6.5 kbar	avP = 6.8 kbar	avP = 6.5 kbar				
py(0.019) gr(0.00028) alm(0.33)		sd = 1.4	sd = 1.3	sd = 1.3				
en(0.23) fs(0.18) mgts(0.031)		fit = 1.16	fit = 1.01	fit = 1.08				
phl(0.089) ann(0.036) an(0.66)								
san(1.0) qtz(1.0)								
92378-1c(M3)	T (°C)	P (kbar)						
	P (kbar)	4.0	5.0	6.0	T (°C)	650	700	750
	G96	700	706	711	NG85	1.6	3.5	5.5
					BK90	3.9	5.5	7.2

700–750 °C at 4–5 kbar (Fig. 3), and the myrmekite assemblage plagioclase–quartz on K-feldspar and biotite–quartz aggregate on biotite in the studied samples may have formed under similar conditions. Thus, the M3 P–T conditions may be constrained as 4–5 kbar and 700–750 °C.

5. Petrogenetic grid in the KFMASH system

The quantitative petrogenetic grids such as P–T and T–X pseudosections calculated for particular bulk compositions in the KFMASH model system have been widely utilized to infer the metamorphic processes and P–T paths that produced the mineral assemblages and reaction textures preserved in metapelites, with the help of the THERMOCALC program (Powell et al., 1998; White et al., 2001). In this case, the mineral assemblages and reaction textures preserved in a structurally early metapelitic granulite (sample 92378-1) in the study region will be quantitatively modeled in the KFMASH system in order to constrain its metamorphic P–T history. Based on the P–T projection of White et al. (2001) constructed for KFMASH metapelites (Fig. 3), P–T and T–X pseudosections are then calculated for the equilibrated mineral assemblages in the sample 92378-1 (Figs. 4 & 5).

5.1. P–T pseudosection

According to volume proportions of equilibrated peak mineral assemblages and corresponding mineral compositions in sample 92378-1, the particular bulk composition for the metapelitic granulite is estimated by THERMOCALC as $\text{H}_2\text{O}:\text{Al}_2\text{O}_3:\text{MgO}:\text{FeO}:\text{K}_2\text{O} = 5.69:27.96:29.90:22.60:13.85$. H_2O was set such that the rock was just water saturated at the wet solidus (Boger and White, 2003). The calculated P–T pseudosection consisting of uni- and multi-variant equilibria is shown in Fig. 4. The reaction textures in the sample suggest that the M1 peak assemblage grt–opx–crd–ksp formed through the univariant partial melting reaction $\text{grt} + \text{bt} = \text{opx} + \text{crd} + \text{ksp} + \text{liq}$ during prograde M1 metamorphism. This univariant reaction seen in the P–T pseudosection indicates that the prograde metamorphic conditions reached 6–8 kbar and

840–880 °C (Fig. 4). The crossing of the univariant reaction $\text{grt} + \text{bt} = \text{opx} + \text{crd} + \text{ksp} + \text{liq}$ suggests that partial melt was produced during an initial prograde heating stage, which is consistent with the observed reaction textures preserved in this metapelitic granulite. The X_{Fe} contours of cordierite in the divariant field (grt opx crd ksp liq) in Fig. 4 indicate that the M2 cordierite corona ($X_{\text{Fe}} = 0.16$), has a higher X_{Mg} than that of peak M1 cordierite ($X_{\text{Fe}} = 0.22$), formed through a cooling and slight increase in pressure (Fig. 4). Therefore, the P–T pseudosection calculations suggest that initial prograde heating resulted in biotite–dehydration melting and the formation of the M1 peak assemblage garnet–orthopyroxene–cordierite–K-feldspar involving a melt phase, whereas post-peak evolution showed a near-isobaric cooling process. This was followed by the development of Mg-rich M2 cordierite coronas around the garnet porphyroblasts. These results are compatible with the average pressure calculation results, indicating a near isobaric cooling process from M1 to M2. As described above, the local M3 cordierite–orthopyroxene symplectite assemblage was suggested to have formed under P–T conditions of 4–5 kbar and 700–750 °C. Thus, M2 to M3 evolution shows a decompression–cooling process (Fig. 4).

5.2. T–X pseudosection

At fixed pressure, a T– X_{Mg} pseudosection can be calculated to show changes in phase relations with changes of temperature and bulk composition over a range of X_{Mg} values. The calculated T– X_{Mg} pseudosection for the metapelitic granulite (sample 92378-1) at 7 kbar is shown in Fig. 5, with an X_{Mg} value of 0.57 for the particular bulk composition used in the P–T pseudosection calculations. With temperature increasing to 860 °C along the bulk composition line, the univariant partial melting reaction would occur and produce a melt phase (Fig. 5). The crossing of the univariant reaction $\text{grt} + \text{bt} = \text{opx} + \text{crd} + \text{ksp} + \text{liq}$ indicates an increase in temperature consistent with the suggestion from the P–T pseudosection. Fig. 5 also suggests that less Mg-rich compositions ($X_{\text{Mg}} < 0.46$) would produce the cordierite-absent trivariant assemblage (grt–opx–ksp–liq) with increasing temperature, whereas more Mg-rich compositions would produce the garnet-absent trivariant assemblage (crd–opx–ksp–

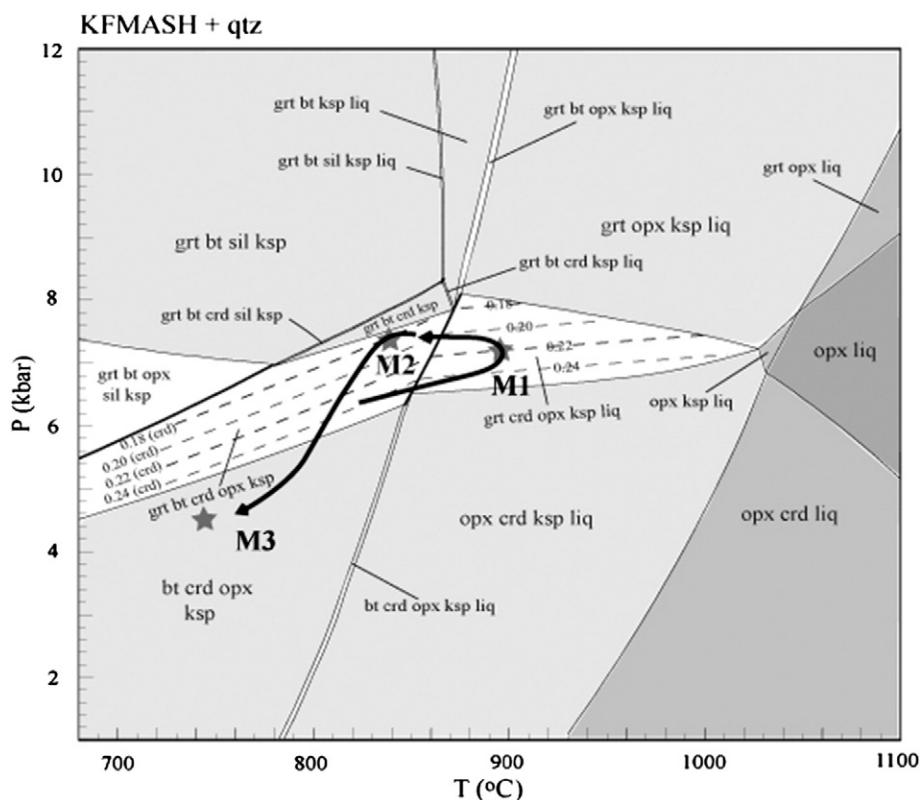


Fig. 4. P–T pseudosection in the KFMASH model system for pelitic granulite (sample 92378-1) with M1 peak assemblage grt–crd–opx–ksp, shows the crossing of the univariant reaction $\text{grt} + \text{bt} = \text{crd} + \text{opx} + \text{ksp} + \text{liq}$ through a prograde heating.

liq). Therefore, the modeled $T-X_{\text{Mg}}$ pseudosection also suggests that sample 92114-1 with cordierite-absent peak assemblage garnet–orthopyroxene–K-feldspar is of a bulk composition richer in Fe, whereas sample 7051 with garnet-absent peak assemblage cordierite–orthopyroxene–K-feldspar possesses a bulk composition richer in Mg.

5.3. Partial melting and leucosome development

In the Larsemann Hills, at least two phases of partial melting events in metapelites (D1–D3) were firstly described by Stüwe and Powell (1989a). Furthermore, they considered that peak M1 garnet and orthopyroxene porphyroblast assemblages with K-feldspar mantles formed through two divariant partial melting reactions in the KFMASH system (Stüwe and Powell, 1989b). Dirks et al. (1993) also described multiple high-grade deformation and in situ partial melting events for this region, and inferred that the apparent decompression textures may have resulted from transient fluxes in water pressure following melt crystallization. Based on the development of minor interstitial K-feldspar in quartz–plagioclase-dominated leucosome assemblages in anatectic metapelitic migmatites in this region, Carson et al. (1997) explained that the leucosomes represent the location of partial melt generation rather than bodies of crystallized melt, and pervasive partial melting and leucosome development occurred as a result of regional decompression of the terrain. However, Fitzsimons (1996) considered that partial melting and leucosome development in the metapelitic migmatites from the adjacent Brattstrand Bluffs coast occurred synchronously with terrain decompression, but was driven mainly by high metamorphic temperature.

The detailed textural observations for the metapelitic granulites in the region presented in this study suggest that the structurally early Al-rich metapelitic granulite (sample 92378-1) preserved the peak M1 assemblage garnet–orthopyroxene–cordierite–K-feldspar, which implies that there was partial melting because the univariant reaction $\text{grt} + \text{bt} = \text{opx} + \text{crd} + \text{ksp} + \text{liq}$ was crossed during the M1 prograde heating stage (Fig. 4). The calculated P–T pseudosection in the KFMASH system shows that post-peak evolution displayed a nearly isobaric cooling in the presence of a melt phase (Fig. 4). However, the boron-bearing metapelite with ~40% leucosomes may suggest higher amounts of melt produced. On the other hand, the reaction textures preserved in the cordierite-absent metapelitic granulite (sample 92114-1) indicate that peak partial melting probably occurred through the crossing of a divariant reaction $\text{grt} + \text{bt} = \text{opx} + \text{ksp} + \text{liq}$. The preservation of peak assemblages without important regression generally implies that some melt loss must have occurred near or during peak metamorphism (White et al., 2001).

6. Discussion

The calculated P–T pseudosection for the early garnet–orthopyroxene–cordierite-bearing metapelitic granulite (sample 92378-1) in the Larsemann Hills, indicates that the M1 peak assemblage garnet–orthopyroxene–cordierite–feldspar formed through the crossing of the univariant partial melting reaction $\text{grt} + \text{bt} = \text{opx} + \text{crd} + \text{ksp} + \text{liq}$ during an initial prograde heating stage, showing a post-peak nearly isobaric cooling anticlockwise P–T path (Fig. 4). The crossing of the above univariant reaction suggests that M1 metamorphic conditions occurred at 6–8 kbar and 840–880 °C (Fig. 4). The M1 pressure

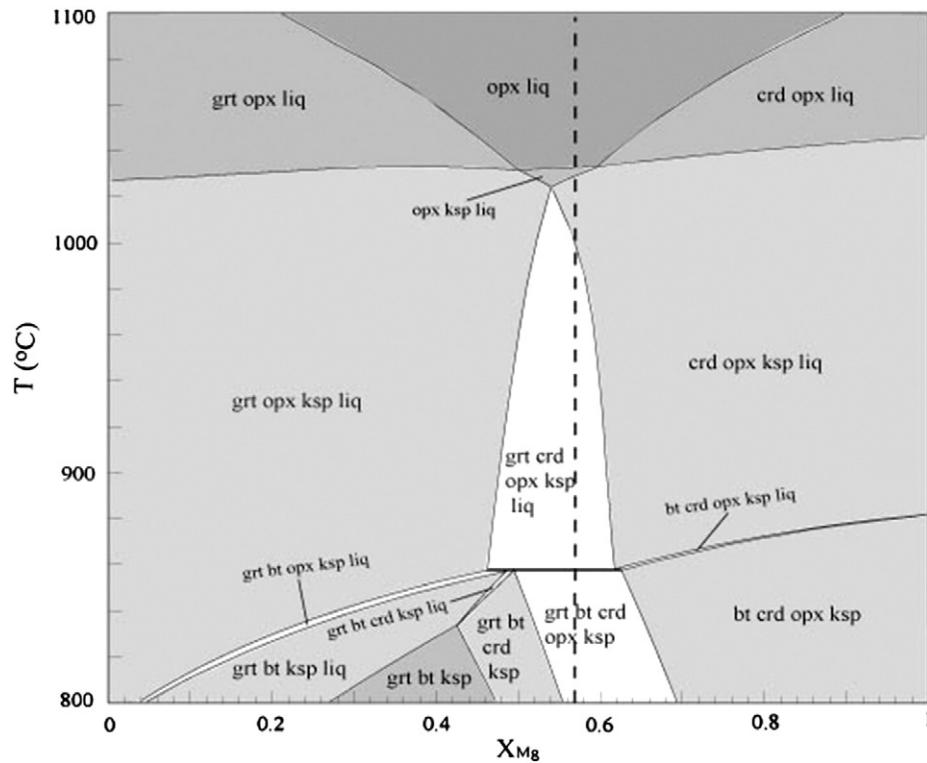


Fig. 5. T - X_{Mg} pseudosection at 7.0 kbar in the KFMASH model system for sample 92378-1 indicates that its bulk composition is of an X_{Mg} value of 0.57 along the dashed line, and phase relations vary with changes in temperature.

estimate for sample 92378-1 similar to that of sample 92114-1 may be from the result of partial re-equilibration of Fe–Mg exchange during cooling. Likewise, that M1 pressure estimate (sample 92378-1) is lower than that of peak M1 assemblage (sample 7051a) may be due to partial reset of Fe–Mg exchange during cooling. Nonetheless, the calculated P–T pseudosection shows that the reaction of formation of the M1 peak assemblage occurred at conditions up to ~8 kbar and ~880 °C, close to M1 P–T estimates of ~9 kbar and ~900 °C for peak M1 assemblage (7051a) in the boron-bearing metapelitic granulite (Table 2). These are consistent with peak M1 conditions of 9.0 kbar and 850 °C and 9.5 kbar and 870 °C derived respectively from grt-sil-pl-qtz geothermobarometry and grt-opx geothermobarometry by Ren et al. (1992) and Tong and Liu (1997) (Fig. 6). M2 peak conditions reached ~7 kbar and 800–850 °C (Table 3), in good agreement with peak M2 conditions of ~7 kbar and ~800 °C reported by Carson et al. (1997). As sapphirine and quartz may constitute part of M2 assemblages (Fig. 2a), peak conditions of 6–7 kbar and 800–860 °C suggested from sapphirine + quartz assemblage by Grew et al. (2006, 2007) should actually reflect peak M2 conditions, which are consistent with the M2 conditions in this study (Fig. 6). P–T estimates for the M3 symplectite assemblage show that M3 metamorphic conditions attained 4–5 kbar and ~700 °C (Table 3). In contrast to the sample 92378-1, P–T results for sample 7051 indicate that M1 post-peak evolution follows a near isothermal decompression process (Fig. 6).

Previous studies considered that the Larsemann Hills region experienced a major ~500 Ma (Pan-African) medium-low pressure high-grade metamorphic event, in response to a single post-peak clockwise decompression P–T path (Carson et al., 1997; Grew et al., 2006, 2007; Ren et al., 1992). However, since the early ~1000 Ma higher P–T metamorphic relics have been recognized from the region (Ren et al., 1992; Tong and Liu, 1997; Tong et al., 2002), this suggests that the previous model involving a single ~500 Ma P–T path needs to be re-evaluated. The above results demonstrate that the

early M1 metamorphic history of the region reflects contrasting P–T evolution paths, while M2 to M3 metamorphic evolution indicates a clockwise decompression-cooling path, which is consistent

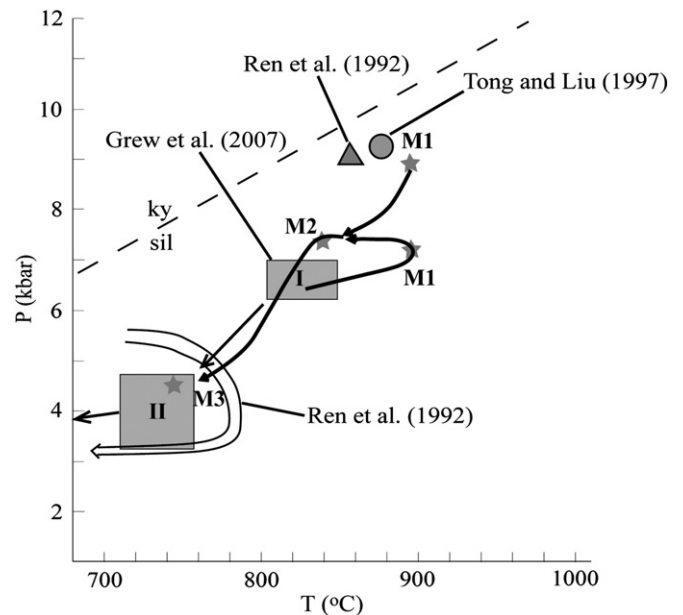


Fig. 6. P–T estimates for M1 and M2 mineral assemblages in the boron-bearing metapelitic granulite (sample 7051) indicate a post-peak decompression, whereas pseudosection modeling for M1 and M2 mineral assemblages in sample 92378-1 shows an initial prograde heating followed by post-peak near isobaric cooling. Also shown are P–T estimates and P–T paths suggested by Ren et al. (1992) and Grew et al. (2007) for the high-grade rocks in the region. The kyanite and sillimanite transition line is after Fig. 3.

with the suggestion of Grew et al. (2006, 2007) (Fig. 6). As described in the previous section, recent SHRIMP zircon U–Pb ages reported by Wang et al. (2008) and Grew et al. (2012) suggest that the early M1 metamorphic event occurred between 1000–900 Ma, while overprinting M2 to M3 metamorphism occurred at ~530 Ma, namely, the integrated P–T paths of the region are actually composed of two separate high-grade structural-metamorphic events, rather than evolving in a single Pan-African high-grade metamorphic event (Carson et al., 1997; Fitzsimons, 1996; Thost et al., 1994). This confirms the initial inference that the metamorphic textures in the paragneisses in the region were the result of overprinting of unrelated metamorphic events (Carson et al., 1995a; Dirks et al., 1993), which is compatible with the suggestion by Vernon (1996) for high-temperature granulite facies terrains involving at least two separate high-grade metamorphic events.

The early M1 contrasting P–T paths showing both a post-peak near isobaric cooling and post-peak near isothermal decompression (Fig. 6) indicate that the early ~1000 Ma P–T paths might involve two different metamorphic evolution processes. A post-peak near isobaric cooling path has been suggested not to be incompatible with a post-peak decompression proposed for other regions of East Antarctica, since different portions of the late Proterozoic (~1000 Ma) high-grade metamorphic belts in East Antarctica may have distinct P–T histories (Thost and Hensen, 1992). For instance, the contrasting late Proterozoic P–T paths involving both a post-peak near isobaric cooling and post-peak near isothermal decompression were generally derived from granulites in the northern Prince Charles Mountains and the Rayner complex (Fitzsimons and Harley, 1992; Halpin et al., 2007). As both sides of the Larsemann Hills have been considered to be of different structural domains (Ren et al., 1992), this implies that the two sides of the region (e.g. the northern Stornes Peninsula and the southern Stornes Peninsula to Broknes Peninsula) may have distinct ~1000 Ma P–T histories. The M1 anticlockwise near isobaric cooling P–T path with initial prograde heating likely corresponds to the prograde D1 thickening event in the region, and may be associated with the intrusion and crystallization of voluminous igneous materials in the crust, probably resulting from some magmatic underplating or the thinning of the mantle lithosphere. This may have provided an important heat input for the prograde M1 high temperature metamorphism, as thinning of the mantle lithosphere may cause rapid heating of thickened crust (Sandiford and Powell, 1991). Such a process is supported by the 970–980 Ma intrusions of the enderbite on Grovnes Peninsula (Wang et al., 2008) and the Blundell Orthogneiss on Stornes Peninsula (Grew et al., 2012). Thus, the prograde M1 metamorphism likely occurred in a tectonic setting of back-arc basin located inboard of an active continental arc, as suggested by Grew et al. (2012).

The M2 P–T conditions are ~7 kbar and 800–850 °C, and M2 to M3 evolution displays a decompression-cooling P–T path (Fig. 6). Mg-rich M2 cordierite coronas on garnet grains and orthopyroxene mantles on biotite reflect overprinting M2 metamorphism, whilst local M3 cordierite–orthopyroxene symplectite on garnet is a result of M3 retrograde decompression-cooling. The M2 conditions are regionally consistent with the Pan-African peak P–T conditions reported from the Rauer Group (Tong and Wilson, 2006). Thus, the overprinting Pan-African metamorphism (M2–M3) may be closely associated with the extensive D2–D3 high-grade transpression deformation in the region, as suggested by Carson et al. (1997). In this case, widespread D2–D3 high-grade transpression and shear resulted in the development of D2–D3 planar high- and low-strain zones in the region, the terrain's exhumation and decompression, partial melting and the development of interstitial K-feldspars (Carson et al., 1997), and the intrusion of the Progress Granite and extensive pegmatite dykes. M2 peak conditions indicate that high-grade transpression occurred at depth of 20–24 km (6–7 kbar).

The Larsemann Hills are located in the central portion of the Prydz Belt in east Antarctica, and clarifying the metamorphic P–T history of the region is critical to the correct reconstruction of the East Gondwana continent and the Rodinia supercontinent. For example, the P–T history of the region and adjacent areas has been considered to have evolved in a single Pan-African high-grade metamorphic event, and the Prydz Belt represents a suture zone that resulted in the final assembly of the East Gondwana continent (Boger et al., 2001; Fitzsimons, 2003; Harley, 2003; Hensen and Zhou, 1997; Zhao et al., 2003). In contrast, others think that the Prydz Belt should represent a polymetamorphic belt (Grew et al., 2012; Liu et al., 2009; Tong et al., 1998, 2002; Wang et al., 2008), and thus it might be associated with an intracontinental reworking (Phillips et al., 2007; Wilson et al., 2007; Yoshida, 2007). The present study, combined with recent chronological data, shows that the region experienced both the early M1 (1000–900 Ma) and second M2–M3 (~530 Ma) metamorphic events, namely, the early M1 P–T evolution history reflects contrasting metamorphic processes, with an overprinting M2–M3 decompression-cooling. Thus, this supports the above second inference that the Prydz Belt actually represents a polymetamorphic belt.

The contrasting M1 metamorphic P–T paths involving a post-peak near isobaric cooling and near isothermal decompression are compatible with those of the northern Prince Charles Mountains and the Rayner complex (Boger and White, 2003; Fitzsimons and Harley, 1992; Halpin et al., 2007; Thost and Hensen, 1992). Recent SHRIMP U–Pb ages of 990–900 Ma recorded from the metamorphic zircon mantles in the paragneisses and orthogneisses in the region (Grew et al., 2012; Wang et al., 2008) and in the high-grade rocks in the eastern Amery Ice Shelf (Liu et al., 2009) are also consistent with the timing of major high-grade metamorphism accompanied by magmatism in the northern Prince Charles Mountains and the Rayner complex (Boger et al., 2000; Carson et al., 2000; Kinny et al., 1997). These indicate that this region and adjacent areas in Prydz Bay might constitute a previously unified late Proterozoic (1000–900 Ma) orogenic belt with the northern Prince Charles Mountains and the Rayner complex, extending to the Eastern Ghats, as suggested by Liu et al. (2009) and Grew et al. (2012). Therefore, the early D1/M1 (1000–900 Ma) high-grade structural-metamorphic event was regionally more extensive than previously envisaged, and might have resulted in the formation of the Indo-Antarctic plate, and hence the assembly of the Rodinia supercontinent.

As stated above, the early Palaeozoic (~530 Ma) Pan-African event in the region and adjacent areas in Prydz Bay belongs to an extensive overprinting high-grade tectonic event, which resulted in the pervasive development of regional planar high-strain shear zones and the intrusion of Pan-African granites and pegmatites (Carson et al., 1997; Sims and Wilson, 1997). In this case, the Pan-African high-grade transpression tectonic event in Prydz Bay actually reflects a significant intracontinental reworking (Phillips et al., 2007, 2009; Wilson et al., 2007; Yoshida, 2007), likely in response to an important intraplate orogen (Boger et al., 2002). This implies that the Prydz Belt actually may represent a Pan-African intraplate tectonic mobile belt. Moreover, the real Pan-African suture zone that led to the formation of the East Gondwana continent may lie inland of Prydz Bay (near Grove Mountains) under continental ice, as suggested recently by Liu et al. (2003, 2009) and Grew et al. (2012).

7. Conclusions

A structurally early grt–opx–crd-bearing Al-rich metapelitic granulite has been recognized from the Larsemann Hills, east Antarctica, with overprinting M2 cordierite corona and M3 opx–

crd symplectite textures. Detailed modeling in the KFMASH system shows that the M1 peak assemblage formed through the crossing of the univariant reaction $\text{grt} + \text{bt} = \text{opx} + \text{crd} + \text{ksp} + \text{liq}$ under conditions of 6–8 kbar and 840–880 °C, with a post-peak near isobaric cooling. Whereas the average P–T calculations for the boron-bearing pelitic granulite indicate that peak M1 conditions reached ~9.0 kbar and ~900 °C, and the overprinting M2 assemblage formed under P–T conditions of ~7.0 kbar and 800–850 °C, reflecting a post-peak near isothermal decompression. P–T estimates show that M3 conditions reached 4–5 kbar and 700–750 °C. These suggest that M1 metamorphic evolution of the region involved contrasting P–T paths, while M2 to M3 evolution was related to a decompression-cooling process. Combined with recent chronological data, we consider that the M1 metamorphic event in the region occurred during the late Proterozoic (1000–900 Ma) Grenvillian tectonic thickening event (D1) accompanied by strong magmatism and the thinning of the mantle lithosphere, and the region occurred as part of a same late Proterozoic (1000–900 Ma) orogenic belt with the northern Prince Charles Mountains and the Rayner complex, and thus was associated with the assembly of the Rodinia supercontinent. Furthermore, the overprinted M2 corona and M3 symplectite textures formed during the early Palaeozoic (~530 Ma) high-grade transpression tectonic D2–D3 events, and were actually a result of a significant Pan-African intracontinental reworking.

Acknowledgments

We thank the leaders and members of the 14th and 27th Chinese National Antarctic Research Expedition (CHINARE) for the logistic support during the 1997–1998 and 2010–2011 Antarctic fieldtrips. The constructive comments on the early manuscript of this paper by Prof. C.J.L. Wilson are very much appreciated. We are also very grateful to Dr. Georg Zellmer for his kind help with a careful correction of English expression on this paper. The valuable comments by Editor Prof. M. Scambelluri and the detailed and critical comments and suggestions by Prof. E.S. Grew and an anonymous reviewer are particularly acknowledged. This study has been supported by the NSFC projects (40976122, 40631004, 41073014), the State Oceanic Administration projects (10/11ZS03-ZS04), and a State Geological Survey project (1212011121006). This is contribution No. IS-1749 from GIG-CAS.

Appendix A. Mineral chemistry

Chemical composition of representative minerals in the studied samples were determined with a CAMECA SX-51 electron microprobe at the Laboratory of Lithospheric Tectonic Evolution, Institute of Geology and Geophysics, Chinese Academy of Sciences, Beijing, operating with an accelerating voltage of 15 kV, a beam current of 20 nA and a beam width of 1–2 μm. Electron microprobe analyses of representative minerals are presented in Appendix B.

Sample 7051: The large Al-rich orthopyroxene porphyroblast is hypersthene in composition, and shows marked composition variations particularly in Al_2O_3 content, in which the Al_2O_3 content in the core (7.75 wt.%) is higher than that in the rim (5.39 wt.%), with corresponding X_{Al} (= Al/2 on the basis of 6 oxygen) values of 0.169 and 0.117 respectively. The X_{Mg} (= Mg / (Mg + Fe^{2+})) value of orthopyroxene in the core is 0.671, lower than that in the rim (0.685), showing an increasing trend from core to rim. The Al_2O_3 content (6.10 wt.%) and X_{Mg} value (0.676) in the fine orthopyroxene lamellae show intermediate compositions between those in the core and the rim. Cordierite also shows a marked zonation in composition, in which the X_{Mg} values vary from 0.880 in the core to 0.848 in

the rim, i.e., a decreasing trend corresponding to the decrease in orthopyroxene X_{Al} from core to rim. Hercynite has a relatively low X_{Mg} value of 0.454, but sapphirine and gedrite have higher X_{Mg} values of 0.784 and 0.753 respectively. However, sapphirine contains a significant Fe^{3+} content of 0.412, indicating that it may have formed in a highly oxidized environment. Biotite in the symplectite has a much higher X_{Mg} value of 0.862 than that (0.791) in the large biotite flake. The prismatic and grandidierite have X_{Mg} values of 0.712 and 0.801 respectively. Plagioclase has a composition of $\text{An}_{20}\text{Ab}_{75}\text{Or}_5$.

Sample 92378-1: Garnet is nearly the most pyrope-rich almandine in the metapelitic granulites in the region and shows a slight variation in composition, with X_{Mg} values decreasing from 0.344 in the core to 0.322 in the rim, and X_{Alm} values increasing from 0.636 in the core to 0.655 in the rim, but X_{Grs} and X_{SpS} values show no appreciable change. Orthopyroxene is of Al-rich hypersthene composition, with an Al_2O_3 content of 6.47 wt.% corresponding to an X_{Al} value of 0.144, and with an X_{Mg} value of 0.598. In contrast, fine-grained orthopyroxene in the corona shows a lower Al_2O_3 content of 4.79 wt.% corresponding to an X_{Al} value of 0.107, and with a lower X_{Mg} value of 0.579. Cordierites have a marked composition difference of X_{Mg} between those in the symplectite and the host, with X_{Mg} values increasing from 0.779 in the host to 0.838 in the symplectite. Biotite has a low X_{Mg} value of 0.590. K-feldspar and plagioclase have the compositions of $\text{An}_0\text{Ab}_7\text{Or}_{93}$ and $\text{An}_{29}\text{Ab}_{70}\text{Or}_1$, respectively.

Sample 92114-1: Garnet is also pyrope-rich almandine and shows slight change in composition, with X_{Mg} values ranging from 0.232 in the garnet inclusion inside the orthopyroxene to 0.269 in the large garnet grain outside the orthopyroxene, and corresponding X_{Alm} values increasing from 0.722 to 0.665 respectively. Orthopyroxene is also of Al-rich hypersthene composition and shows some variation in Al_2O_3 content, which indicates an increase from 5.01 wt.% in the core to 5.61 wt.% in the rim, with corresponding X_{Al} values of 0.115 and 0.128, respectively, while the late orthopyroxene mantle on biotite shows a lower Al_2O_3 content (4.69 wt.%) with a corresponding X_{Al} value of 0.106, but X_{Mg} values have no apparent variation. K-feldspar has a composition of $\text{An}_7\text{Ab}_{12}\text{Or}_{81}$. Plagioclase inclusions in orthopyroxene and plagioclase outside orthopyroxene are $\text{An}_{47}\text{Ab}_{12}\text{Or}_2$ and $\text{An}_{53}\text{Ab}_{45}\text{Or}_2$, respectively, indicating that Ca content increases and Na content decreases from the inclusions to the matrix. Biotite shows a similar X_{Mg} value of 0.581 to that from sample 92378-1. Late hercynite has a low X_{Mg} value of 0.217.

Appendix B

Electron microprobe data of representative minerals in the orthopyroxene-bearing metapelitic granulites from the study region. Note: All Fe as FeO. Fe_2O_3 was estimated via charge balance calculation. Abbreviations: crd(c), cordierite core; crd(r), cordierite rim; opx(h), orthopyroxene host; opx(s), orthopyroxene lamellae; opx(r), orthopyroxene rim; prs, prismatic; gdd, grandidierite; bt1, peak biotite; bt2, biotite in symplectite; hc, hercynite; grt(c), garnet core; grt(r), garnet rim; opx1, peak orthopyroxene; opx3, orthopyroxene in symplectite or mantle; crd1, peak cordierite; crd2, cordierite in corona; grt(i), garnet inclusion in opx; grt(o), garnet outside opx; opx(c), orthopyroxene core; pl(i), plagioclase inclusion in opx; pl(o), plagioclase outside opx; $X_{\text{Mg}} = \text{Mg} / (\text{Fe}^{2+} + \text{Mg})$; $X_{\text{Al}} = \text{Al} / 2$; $X_{\text{An}} = \text{Ca} / (\text{Ca} + \text{Na} + \text{K})$; $X_{\text{Ab}} = \text{Na} / (\text{Ca} + \text{Na} + \text{K})$; $X_{\text{Or}} = \text{K} / (\text{Ca} + \text{Na} + \text{K})$; $X_{\text{Alm}} = \text{Fe}^{2+} / (\text{Fe}^{2+} + \text{Mg} + \text{Ca} + \text{Mn})$; $X_{\text{Grs}} = \text{Ca} / (\text{Fe}^{2+} + \text{Mg} + \text{Ca} + \text{Mn})$; $X_{\text{Prp}} = \text{Mg} / (\text{Fe}^{2+} + \text{Mg} + \text{Ca} + \text{Mn})$; $X_{\text{SpS}} = \text{Mn} / (\text{Fe}^{2+} + \text{Mg} + \text{Ca} + \text{Mn})$.

Appendix B

	7051													92378-1		
	crd (c)	crd (r)	opx(h)	opx(s)	opx(r)	hc	spr	ged	prs	gdd	pl	bt1	bt2	grt(c)	grt(r)	opx1
SiO ₂	49.60	49.04	48.53	47.25	49.97	0.05	12.01	40.25	29.89	20.31	62.34	38.62	41.10	38.26	38.46	47.79
TiO ₂	0.00	0.00	0.02	0.82	0.14	0.03	0.06	0.56	0.25	0.05	0.06	3.22	0.16	0.03	0.02	0.11
Al ₂ O ₃	35.41	35.37	7.75	6.10	5.39	60.27	60.65	20.38	40.40	51.14	22.22	14.05	13.79	21.20	21.22	6.47
Cr ₂ O ₃	0.00	0.00	0.00	0.07	0.03	0.47	0.17	0.04	0.03	0.03	0.00	0.06	0.02	0.04	0.09	0.03
Fe ₂ O ₃	0.78	0.99	2.81	7.09	2.26	3.49	4.52	4.61	0.00	0.14	1.00	0.00	0.00	1.68	0.43	3.58
FeO	2.80	3.56	19.00	18.43	18.76	23.96	7.33	10.67	10.17	5.16	0.00	9.10	6.59	29.13	30.16	22.89
MnO	0.00	0.10	0.14	0.13	0.08	0.04	0.03	0.14	0.08	0.04	0.00	0.00	0.07	0.37	0.48	0.15
MgO	11.56	11.11	21.70	21.57	22.90	11.20	14.97	18.24	14.79	11.55	0.00	19.30	23.04	8.56	8.05	19.10
CaO	0.00	0.01	0.11	0.08	0.07	0.00	0.00	0.25	0.05	0.00	4.23	0.00	0.06	0.79	0.79	0.07
Na ₂ O	0.02	0.07	0.02	0.02	0.02	0.00	0.02	3.14	0.09	0.00	8.52	0.28	0.15	0.00	0.00	0.01
K ₂ O	0.04	0.02	0.00	0.01	0.00	0.01	0.01	0.02	0.00	0.01	0.84	9.91	10.00	0.00	0.00	0.01
ZnO																
Totals	100.21	100.27	100.08	101.57	99.62	99.52	99.77	98.30	98.96	88.28	98.36	95.55	94.98	100.07	99.70	100.21
O	18	18	6	6	6	4	20	23	20	7.5	8	22	22	12	12	6
Si	4.897	4.865	1.792	1.746	1.848	0.001	1.454	5.708	3.669	0.998	2.809	5.638	5.896	2.976	3.006	1.802
Ti	0.000	0.000	0.001	0.023	0.004	0.001	0.005	0.060	0.027	0.002	0.002	0.354	0.018	0.002	0.001	0.003
Al	4.122	4.136	0.337	0.266	0.235	1.920	8.658	3.407	5.834	2.956	1.180	2.417	2.332	1.944	1.955	0.288
Cr	0.000	0.000	0.000	0.002	0.001	0.010	0.016	0.004	0.003	0.001	0.000	0.007	0.002	0.002	0.006	0.001
Fe ³⁺	0.058	0.074	0.078	0.197	0.063	0.071	0.412	0.492	0.000	0.000	0.005	0.110	0.000	0.099	0.025	0.102
Fe ²⁺	0.231	0.295	0.587	0.569	0.580	0.542	0.743	1.266	1.102	0.211	0.000	1.108	0.790	1.895	1.971	0.722
Mn	0.000	0.008	0.004	0.004	0.003	0.001	0.003	0.017	0.008	0.002	0.000	0.000	0.008	0.024	0.032	0.005
Mg	1.701	1.642	1.195	1.188	1.262	0.451	2.702	3.855	2.725	0.851	0.000	4.199	4.927	0.992	0.938	1.074
Ca	0.000	0.001	0.005	0.003	0.003	0.000	0.000	0.038	0.007	0.000	0.204	0.000	0.009	0.066	0.066	0.003
Na	0.004	0.013	0.001	0.001	0.001	0.000	0.005	0.863	0.005	0.000	0.744	0.078	0.041	0.000	0.000	0.001
K	0.005	0.003	0.000	0.001	0.000	0.000	0.002	0.004	0.000	0.000	0.048	1.844	1.831	0.000	0.000	0.000
Zn																
Sum	11.018	11.04	4.000	4.000	4.000	2.997	14.000	15.714	13.380	5.021	4.993	15.758	15.85	8.000	8.000	4.000
X _{Mg}	0.880	0.848	0.671	0.676	0.685	0.454	0.784	0.753	0.712	0.801		0.791	0.862	0.344	0.322	0.598
X _{Al}			0.169	0.133	0.117											0.144
X _{An}												0.205				
X _{Ab}												0.747				
X _{Or}												0.048				
X _{Grs}														0.022	0.022	
X _{Prp}														0.333	0.312	
X _{Sps}														0.008	0.011	
X _{Alm}														0.636	0.655	

References

- Boger, S.D., White, R.W., 2003. The metamorphic evolution of metapelitic granulites from Radok Lake, northern Prince Charles Mountains, east Antarctica: evidence for an anticlockwise P–T path. *Journal of Metamorphic Geology* 21, 1–14.
- Boger, S.D., Carson, C.J., Wilson, C.J.L., Fanning, C.M., 2000. Neoproterozoic deformation in the Radok Lake region of the northern Prince Charles Mountains, east Antarctica: evidence for a single protracted orogenic event. *Precambrian Research* 104, 1–24.
- Boger, S.D., Wilson, C.J.L., Fanning, C.M., 2001. Early Paleozoic tectonism within the East Antarctic craton: the final suture between east and west Gondwana? *Geology* 29, 463–466.
- Boger, S.D., Carson, C.J., Fanning, C.M., Hergt, J.M., Wilson, C.J.L., Woodhead, J.D., 2002. Pan-African intraplate deformation in the northern Prince Charles Mountains, east Antarctica. *Earth and Planetary Science Letters* 195, 195–210.
- Brey, G.T., Kohler, T., 1990. Geothermobarometry in four phase Iherolites, part II: new thermobarometers, and practical assessment of existing thermobarometers. *Journal of Petrology* 31, 1353–1378.
- Carson, C.J., Grew, E.S., 2007. Geology of the Larsemann Hills region, Antarctica, First Edition, 1:25 000 scale map, Canberra, Geoscience Australia.
- Carson, C.J., Dirks, P.H.G.M., Hand, M., Sims, J.P., Wilson, C.J.L., 1995a. Compressional and extensional tectonics in low-medium pressure granulites from the Larsemann Hills, East Antarctica. *Geological Magazine* 132, 151–170.
- Carson, C.J., Hand, M., Dirks, P.H.G.M., 1995b. Stable coexistence of grandierite and kornepirine during medium pressure granulite facies metamorphism. *Mineralogical Magazine* 59, 327–339.
- Carson, C.J., Fanning, C.M., Wilson, C.J.L., 1996. Timing of the Progress Granite, Larsemann Hills: evidence for Early Palaeozoic orogenesis within the east Antarctic Shield and implications for Gondwana assembly. *Australian Journal of Earth Sciences* 43, 539–553.
- Carson, C.J., Powell, R., Wilson, C.J.L., Dirks, P.H.G.M., 1997. Partial melting during tectonic exhumation of a granulite terrane: an example from the Larsemann Hills, East Antarctica. *Journal of Metamorphic Geology* 15, 105–126.
- Carson, C.J., Boger, S.D., Fanning, C.M., Wilson, C.J.L., Thost, D.E., 2000. SHRIMP U–Pb geochronology from Mount Kirby, northern Prince Charles Mountains, East Antarctica. *Antarctic Science* 12, 429–442.
- Cooper, M.A., Hawthorne, F.C., Grew, E.S., 2009. The crystal chemistry of the kornepirine-prismatic series. I. Crystal structure and site populations. *The Canadian Mineralogist* 47, 233–262.
- Dirks, P.H.G.M., Hand, M., 1995. Clarifying temperature–pressure paths via structures in granulite from the Bolingen Islands, Antarctica. *Australian Journal of Earth Sciences* 42, 157–172.
- Dirks, P.H.G.M., Wilson, C.J.L., 1995. Crustal evolution of the East Antarctic mobile belt in Prydz Bay. *Continental collision at 500 Ma? Precambrian Research* 75, 189–207.
- Dirks, P.H.G.M., Carson, C.J., Wilson, C.J.L., 1993. The deformation history of the Larsemann Hills, Prydz Bay: the importance of the Pan-African (500 Ma) in East Antarctica. *Antarctic Science* 5, 179–193.
- Fitzsimons, I.C.W., 1996. Metapelitic migmatites from Brattstrand Bluffs, east Antarctica – metamorphism, melting and exhumation of the mid-crust. *Journal of Petrology* 37, 395–414.
- Fitzsimons, I.C.W., 1997. The Brattstrand paragneiss and the Sostrene orthogneiss: a review of Pan-African metamorphism and Grenvillian relics in southern Prydz Bay. In: Ricci, C.A. (Ed.), *The Antarctic Region: Geological Evolution and Processes*. Terra Antarctica Publ. Siena, pp. 121–130.
- Fitzsimons, I.C.W., 2003. Proterozoic basement provinces of southern and southwestern Australia, and their correlation with Antarctica. In: Yoshida, M., et al. (Eds.), *Proterozoic East Gondwana: Supercontinent Assembly and Breakup*. Geological Society London Special Publication, 206, pp. 93–130.
- Fitzsimons, I.C.W., Harley, S.L., 1991. Geological relationships in high-grade gneiss of the Brattstrand Bluffs coastline, Prydz Bay, east Antarctica. *Australian Journal of Earth Sciences* 38, 497–519.
- Fitzsimons, I.C.W., Harley, S.L., 1992. Mineral reaction textures in high-grade gneisses: evidence for contrasting pressure–temperature paths in the Proterozoic complex of east Antarctica. In: Yoshida, Y., et al. (Eds.), *Recent Progress in Antarctic Earth Science*. Terrapub, Tokyo, pp. 103–111.
- Fitzsimons, I.C.W., Kinny, P.D., Harley, S.L., 1997. Two stages of zircon and monazite growth in anatectic leucogneiss: SHRIMP constraints on the duration and intensity of Pan-African metamorphism in Prydz Bay, East Antarctica. *Terra Nova* 9, 47–51.
- Ganguly, J., Cheng, W., Tirone, M., 1996. Thermodynamics of aluminosilicate garnet solid solution: new experimental data, an optimized model, and thermometric applications. *Contributions to Mineralogy and Petrology* 126, 137–151.
- Grew, E.S., Armbruster, T., Medenbach, O., Yates, M.G., Carson, C.J., 2006. Stornesite-(Y), (Y, Ca)₂Na₆(Ca, Na)₈(Mg, Fe)₄₃(PO₄)₃₆, the first terrestrial Mg-dominant member of the fyllowite group, from granulite-facies paragneiss in the Larsemann Hills, Prydz Bay, East Antarctica. *American Mineralogist* 91, 1412–1424.
- Grew, E.S., Armbruster, T., Medenbach, O., Yates, M.G., Carson, C.J., 2007. Chopinite, [(Mg, Fe)₃](PO₄)₂, a new mineral isostructural with sarcopside, from a fluorapatite

92114-1															
opx3	crd1	crd2	ksp	pl	bt	grt(i)	grt(o)	opx(c)	opx(r)	opx2	ksp	pl(i)	pl(o)	bt	hc
50.26	49.63	50.03	64.25	60.98	37.26	36.71	36.77	45.99	46.45	48.87	63.33	56.78	54.92	36.29	0.05
0.00	0.00	0.00	0.01	0.02	3.69	0.05	0.01	0.10	0.17	0.14	0.02	0.03	0.03	5.79	0.00
4.79	33.39	33.24	18.50	24.42	14.61	21.07	21.10	5.01	5.61	4.69	19.42	26.29	28.02	13.73	56.11
0.19	0.08	0.00	0.02	0.00	0.00	0.05	0.00	0.02	0.00	0.00	0.00	0.00	0.00	0.05	0.69
0.00	1.45	1.11	0.07	0.06	0.00	0.24	0.53	5.87	4.42	0.87	0.00	0.00	0.00	0.00	5.20
25.14	5.22	4.01	0.00	0.00	17.01	32.11	31.04	25.21	25.73	27.52	0.04	0.10	0.10	16.52	29.83
0.08	0.05	0.06	0.00	0.00	0.00	2.01	1.90	0.58	0.62	0.40	0.00	0.04	0.00	0.01	0.21
19.43	10.34	11.63	0.00	0.00	13.72	5.44	6.41	16.24	16.31	17.08	0.00	0.00	0.00	12.87	4.64
0.04	0.01	0.00	0.01	6.08	0.00	1.67	1.77	0.18	0.20	0.13	1.45	9.53	10.86	0.00	0.00
0.00	0.03	0.00	0.73	8.21	0.00	0.00	0.00	0.02	0.00	0.00	1.35	5.69	5.14	0.05	0.11
0.00	0.02	0.00	15.08	0.13	9.68	0.01	0.00	0.01	0.00	0.01	13.66	0.36	0.35	9.53	0.00
															4.15
99.93	100.23	100.09	98.68	99.90	95.97	99.36	99.53	99.23	99.51	99.62	99.27	98.82	99.42	94.84	100.99
6	18	18	8	8	22	12	12	6	6	6	8	8	8	22	4
1.893	4.965	4.979	2.994	2.713	5.576	2.945	2.932	1.796	1.802	1.877	2.935	2.579	2.491	5.513	0.001
0.000	0.000	0.000	0.000	0.00	0.416	0.003	0.000	0.003	0.005	0.004	0.001	0.001	0.001	0.662	0.000
0.213	3.938	3.900	1.016	1.281	2.578	1.992	1.983	0.231	0.257	0.212	1.061	1.407	1.498	2.459	1.874
0.006	0.006	0.000	0.001	0.000	0.000	0.003	0.000	0.001	0.000	0.000	0.000	0.000	0.000	0.006	0.015
0.000	0.109	0.083	0.002	0.002	0.000	0.015	0.032	0.172	0.129	0.025	0.000	0.000	0.000	0.000	0.111
0.792	0.437	0.334	0.000	0.000	2.130	2.154	2.070	0.823	0.835	0.884	0.001	0.004	0.004	2.099	0.707
0.003	0.004	0.005	0.000	0.000	0.000	0.136	0.128	0.019	0.020	0.013	0.000	0.002	0.000	0.002	0.005
1.091	1.542	1.727	0.000	0.000	3.062	0.651	0.762	0.946	0.943	0.987	0.000	0.000	0.000	2.915	0.196
0.002	0.001	0.000	0.000	0.290	0.000	0.144	0.151	0.008	0.009	0.005	0.072	0.464	0.528	0.000	0.000
0.000	0.006	0.000	0.066	0.708	0.000	0.000	0.000	0.001	0.000	0.000	0.121	0.501	0.452	0.015	0.006
0.000	0.003	0.000	0.897	0.007	1.848	0.001	0.000	0.000	0.000	0.000	0.808	0.021	0.020	1.847	0.000
															0.087
3.998	11.012	11.029	4.978	5.002	15.610	8.044	8.058	4.000	4.000	4.000	4.999	4.979	4.994	15.520	3.002
0.579	0.779	0.838			0.590	0.232	0.269	0.535	0.531	0.528				0.581	0.217
0.107								0.115	0.128	0.106					
			0.00	0.289							0.072	0.471	0.528		
			0.069	0.70							0.121	0.508	0.452		
			0.931	0.007							0.807	0.021	0.020		
						0.048	0.049								
						0.218	0.245								
						0.046	0.041								
						0.722	0.665								

- segregation in granulite-facies paragneiss, Larsemann Hills, Prydz Bay, East Antarctica. *European Journal of Mineralogy* 19, 229–245.
- Grew, E.S., Carson, C.J.L., Christy, A.G., Maas, R., Yaxley, G.M., Boger, S.D., Fanning, C.M., 2012. New constraints from U–Pb, Lu–Hf and Sm–Nd isotopic data on the timing of sedimentation and felsic magmatism in the Larsemann Hills, Prydz Bay, east Antarctica. *Precambrian Research* 206, 87–108.
- Halpin, J.A., Clarke, G.L., White, R.W., Kelsey, D., 2007. Contrasting P–T paths for Neoproterozoic metamorphism in McRobertson and Kemp Lands, east Antarctica. *Journal of Metamorphic Geology* 25, 683–701.
- Harley, S.L., 2003. Archaean–Cambrian crustal development of East Antarctica: metamorphic characteristics and tectonic implications. In: Yoshida, M., et al. (Eds.), *Proterozoic East Gondwana: Supercontinent Assembly and Breakup*. Geological Society London Special Publication, 206, pp. 203–230.
- Harley, S.L., Fitzsimons, I.C.W., 1991. Pressure–temperature evolution of metapelitic granulites in a polymetamorphic terrane: the Rauer Group, East Antarctica. *Journal of Metamorphic Geology* 9, 231–243.
- Hensen, B.J., Zhou, B., 1995. A Pan African granulite facies metamorphic episode in Prydz Bay, Antarctica: evidence from Sm–Nd garnet dating. *Australian Journal of Earth Sciences* 42, 249–258.
- Hensen, B.J., Zhou, B., 1997. East Gondwana amalgamation by Pan-African collision? Evidence from Prydz Bay, east Antarctica. In: Ricci, C.A. (Ed.), *The Antarctic Region: Geological Evolution and Processes*. Terra Antarctica Publ, Siena, pp. 115–119.
- Hensen, B.J., Zhou, B., Thost, D.E., 1995. Are reaction textures reliable guides to metamorphic histories? Timing constraints from garnet Sm–Nd chronology for ‘decompression’ textures in granulites from Sostrene Island, Prydz Bay, Antarctica. *Geological Journal* 30, 261–271.
- Holland, T.J.B., Powell, R., 1998. An internally-consistent thermodynamic data set for phases of petrological interest. *Journal of Metamorphic Geology* 16, 309–394.
- Holland, T.J.B., Powell, R., 2001. Calculations of phase relations involving haplogranitic melts using an internally consistent thermodynamic dataset. *Journal of Petrology* 42, 673–683.
- Kelsey, E., Wade, B.P., Collins, A.S., Hand, M., Sealing, C.R., Netting, A., 2008. Discovery of a Neoproterozoic basin in the Prydz belt in East Antarctica and its implications for Gondwana assembly and ultrahigh temperature metamorphism. *Precambrian Research* 161, 355–388.
- Kinny, P.D., 1998. Monazite U–Pb ages from east Antarctic granulites: comparisons with zircon U–Pb and garnet Sm–Nd ages. *Geological Society of Australia* 49, 250 (abst).
- Kinny, P.D., Black, L.P., Sheraton, J.W., 1997. Zircon U–Pb ages and geochemistry of igneous and metamorphic rocks from the northern Prince Charles Mountains, Antarctica. *AGSO Journal of Australian Geology and Geophysics* 16, 637–654.
- Liu, X., Zhao, Y., Liu, X., Yu, L., 2003. Geology of the Grove Mountains in East Antarctica – new evidence for the final suture of Gondwana land. *Science in China, Series D* 46, 305–319.
- Liu, X., Zhao, Y., Song, B., Liu, J., Cui, J., 2009. SHRIMP U–Pb zircon geochronology of high-grade rocks and charnockites from the eastern Amery Ice Shelf and southwestern Prydz Bay, East Antarctica: constraints on Late Mesoproterozoic to Cambrian tectonothermal events related to supercontinent assembly. *Gondwana Research* 16, 342–361.
- Nickel, K.G., Green, D.H., 1985. Empirical geothermobarometry for garnet peridotites and implications for the nature of the lithosphere, kimberlites and diamonds. *Earth and Planetary Science Letters* 73, 158–170.
- Phillips, G., Wilson, C.J.L., Phillips, D., Szczepanski, S., 2007. Thermochronological (Ar/Ar) evidence of early Palaeozoic basin inversion within the southern Prince Charles Mountains, east Antarctica: implications for East Gondwana. *Journal of Geological Society London* 164, 771–784.
- Phillips, G., Kelsey, D., Corvino, A.F., Dutch, R.A., 2009. Continental reworking during overprinting orogenic events, southern Prince Charles Mountains, East Antarctica. *Journal of Petrology* 50, 2017–2041.
- Powell, R., Holland, T.J.B., 1994. Optimal geothermometry and geobarometry. *American Mineralogist* 79, 120–133.
- Powell, R., Holland, T.J.B., Worley, B., 1998. Calculating phase diagrams involving solid solutions via non-linear equations, with examples using THERMOCALC. *Journal of Metamorphic Geology* 16, 577–588.
- Ren, L., Liu, X., 1994. Occurrence of the assemblage grandierite, kornerupine, and tourmaline in Antarctica. *Antarctic Research* 6, 1–7 (in Chinese with English abstract).
- Ren, L., Zhao, Y., 2004. Occurrence of prismatine at the Zhongshan Station area, East Antarctica, and the changes of its definition. *Acta Petrologica Sinica* 20, 759–763.
- Ren, L., Zhao, Y., Liu, X., Chen, T., 1992. Re-examination of the metamorphic evolution of the Larsemann Hill, East Antarctica. In: Yoshida, Y., et al. (Eds.), *Recent Progress in Antarctic Earth Science*. Terrapub, Tokyo, pp. 145–153.
- Ren, L., Wang, Y., Zhao, Y., 2008. Sapphirine in the high-grade quartzofeldspathic gneiss of the Larsemann Hills, East Antarctica. *Chinese Journal of Polar Science* 19, 1–13.
- Sandiford, M., Powell, R., 1991. Some remarks on high-temperature–low-pressure metamorphism in convergent orogens. *Journal of Metamorphic Geology* 9, 333–340.
- Sheraton, J.W., Black, L.P., McCulloch, M.T., 1984. Regional geochemical and isotopic characteristic of high-grade metamorphic of the Prydz Bay area: the extent of Proterozoic

- reworking of Archaean continental crust in East Antarctica. *Precambrian Research* 26, 169–198.
- Sims, J.P., Wilson, C.J.L., 1997. Strain localisation and texture development in a granulite-facies shear zone — the Rauer Group, east Antarctica. In: Ricci, C.A. (Ed.), *The Antarctic Region: Geological Evolution and Processes*. Terra Antarctica Publ, Siena, pp. 131–138.
- Stüwe, K., Powell, R., 1989a. Low-pressure granulite facies metamorphism in the Larsemann Hills area, East Antarctica; petrology and tectonic implications for the evolution of the Prydz Bay area. *Journal of Metamorphic Geology* 7, 465–483.
- Stüwe, K., Powell, R., 1989b. Metamorphic segregations associated with garnet and orthopyroxene porphyroblast growth: two examples from the Larsemann Hills, East Antarctica. *Contributions to Mineralogy and Petrology* 103, 523–530.
- Stüwe, K., Braun, H.-M., Peer, H.-M., 1989. Geology and structure of the Larsemann Hills area, Prydz Bay, East Antarctica. *Australian Journal of Earth Sciences* 36, 219–241.
- Thost, D.E., Hensen, B.J., 1992. Gneisses of the Porthos and Athos ranges, northern Prince Charles mountains, east Antarctica: constraints on the prograde and retrograde P–T path. In: Yoshida, Y., et al. (Eds.), *Recent Progress in Antarctic Earth Science*. Terrapub, Tokyo, pp. 93–102.
- Thost, D.E., Hensen, B.J., Motoyoshi, Y., 1991. Two-stage decompression in garnet-bearing mafic granulites from Søstrene Island, Prydz Bay, East Antarctica. *Journal of Metamorphic Geology* 9, 245–256.
- Thost, D.E., Hensen, B.J., Motoyoshi, Y., 1994. The geology of a rapidly uplifted medium and low-pressure granulite terrane of Pan-African age: the Bolingen Islands, Prydz Bay, East Antarctica. *Petrology* 2, 293–316.
- Tong, L., Liu, X., 1997. The prograde metamorphism of the Larsemann Hills: evidence for an anticlockwise P–T path. In: Ricci, C.A. (Ed.), *The Antarctic Region: Geological Evolution and Processes*. Terra Antarctica Publ, Siena, pp. 105–114.
- Tong, L., Wilson, C.J.L., 2006. Tectonothermal evolution of the ultrahigh temperature metapelites in the Rauer Group, east Antarctica. *Precambrian Research* 149, 1–20.
- Tong, L., Liu, X., Zhang, L., Chen, H., Chen, F., Wang, Y., Ren, L., 1998. The Ar–Ar ages of hornblendes in Grt–Pl-bearing amphibolite from the Larsemann Hills, East Antarctica and their geological implications. *Chinese Journal of Polar Sciences* 9, 79–91.
- Tong, L., Wilson, C.J.L., Liu, X., 2002. A high-grade event of 1100 Ma preserved within the 500 Ma mobile belt of the Larsemann Hills, east Antarctica: further evidence from 40Ar–39Ar dating. *Terra Antarctica* 9, 73–86.
- Vernon, R.H., 1996. Problems with inferring P–T–t paths in low-P granulite facies rocks. *Journal of Metamorphic Geology* 14, 143–153.
- Wang, Y., Tong, L., Liu, D., 2007. Zircon U–Pb ages from an ultra-high temperature metapelite, Rauer Group, east Antarctica: implications for overprints by Grenvillian and Pan-African events. <http://dx.doi.org/10.3133/of2007-1047.srp023> (USGS OF-2007-1047, Short Res. Paper 023).
- Wang, Y., Liu, D., Chung, S.-L., Tong, L., Ren, L., 2008. SHRIMP zircon age constraints from the Larsemann Hills region, Prydz Bay, for a late Mesoproterozoic to early Neoproterozoic tectono-thermal event in east Antarctica. *American Journal of Sciences* 308, 573–617.
- White, R.W., Powell, R., Holland, T.J.B., 2001. Calculation of partial melting equilibria in the system Na₂O–CaO–FeO–MgO–Al₂O₃–SiO₂–H₂O (NCKFMASH). *Journal of Metamorphic Geology* 19, 139–153.
- Wilson, C.J.L., Quinn, C., Tong, L., Phillips, D., 2007. Early Palaeozoic intracratonic shears and post-tectonic cooling in the Rauer Group, Prydz Bay, East Antarctica constrained by ⁴⁰Ar/³⁹Ar thermochronology. *Antarctic Sciences* 19, 339–353.
- Yoshida, W., 2007. Geochronological data evaluation: implications for the Proterozoic tectonics of East Antarctica. *Gondwana Research* 12, 228–241.
- Zhang, L., Tong, L., Liu, X., Scharer, U., 1996. Conventional U–Pb age of the high-grade metamorphic rocks in the Larsemann Hills, East Antarctica. In: Pang, Z., et al. (Eds.), *Advances in Solid Earth Sciences*. Science Press, Beijing, pp. 27–35.
- Zhao, Y., Song, B., Wang, Y., Ren, L., Li, J., Chen, T., 1992. Geochronology of the late granite in the Larsemann Hills, East Antarctica. In: Yoshida, Y., et al. (Eds.), *Recent Progress in Antarctic Earth Science*. Terra Scientific Publ. Company, Tokyo, pp. 153–169.
- Zhao, Y., Liu, X., Song, B., Zhang, Z., Li, J., Yao, Y., Wang, Y., 1995. Constraints on stratigraphic age of metasedimentary rocks of the Larsemann Hills, East Antarctica: possible implication for Neoproterozoic tectonics. *Precambrian Research* 75, 175–188.
- Zhao, Y., Liu, X.H., Liu, X.C., Song, B., 2003. Pan-African events in Prydz Bay, East Antarctica, and their implications for East Gondwana tectonics. In: Yoshida, M., et al. (Eds.), *Proterozoic East Gondwana: Supercontinent Assembly and Breakup*. Geological Society London Special Publication, 206, pp. 231–245.